# Multiscale three-dimensional stress analysis of voids clusters for the modelling of degenerated graphite in cast iron



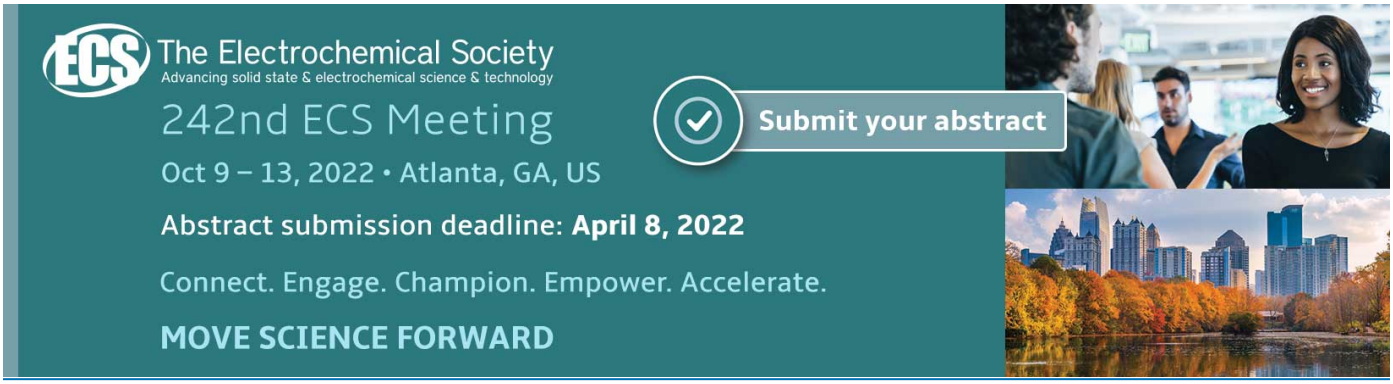

# Multiscale three-dimensional stress analysis of voids clusters for the modelling of degenerated graphite in cast iron

**R Rizzoni, P Livieri and R Tovo**

Department of Engineering, University of Ferrara, Via Saragat 1, 44122 Ferrara, Italy

E-mail: raffaella.rizzoni@unife.it

**Abstract**. We propose a multiscale three-dimensional model for the stress analysis of a cluster of degenerated graphite in spheroidal cast iron. The model allows to study the effect of graphite microstructure on the average stress distribution inside the cluster. At the microscale, precipitates of degenerated graphite are modelled as spheroidal voids. At the mesoscale, clusters of degenerated graphite are viewed as spheroidal inclusions made of equivalent porous elastic material. The equivalent elastic properties of the porous material are calculated using an approach proposed by Tandon and Weng and based on Eshelby's equivalent principle and the Mori-Tanaka's estimate. FE simulations at the microscale and at the mesoscale are performed in order to numerically validate the multiscale model.

## 1. Introduction

In cast iron, experimental evidence of correlation between microstructure morphology and mechanical properties is largely reported, see [1-3] and the references therein. Degenerated graphite occurs in heavy section and for long solidification times, and it is a critical defect, reducing the mechanical properties of the parts [4,5]. The effects of graphite degeneration on the mechanical properties of cast iron are very challenging to model, even in a linear elastic framework. Simplifying approaches treating single defects as elliptical/ellipsoidal inclusions are commonly explored in the literature [6-9].

In a two-dimensional setting, a first proposal of multiscale hierarchical approach for the description of the behaviour of degenerated graphite was first presented in [10,11]. In this summary, we extend the previous multiscale analysis to the three-dimensional case. In particular, at the microscopic scale, graphite precipitates are modelled as spheroidal voids, randomly oriented and homogenously distributed in an elastic isotropic matrix. At this scale, the effective properties of the porous equivalent material are evaluated by using Mori-Tanaka's (MT) estimate for composites as proposed by Tandon and Weng [12]. At the mesoscale, a degenerated graphite cluster is modelled as a single spheroidal inclusion embedded into the elastic isotropic matrix, and made of the equivalent porous material characterized at the microscale. Eshelby's fundamental solution [13-15] is then applied to describe the dependence of the stress state, internal to the cluster of degenerated graphite, on the following basic microstructure parameters: the density of graphite particles, their aspect ratio, the orientation and aspect ratio of the cluster of degenerated graphite.

Comparison with the results obtained by a finite element (FE) analysis for several types of defect distributions are also discussed. At the microscale, the effective properties of a cube containing several random distributions of spheroidal voids are calculated by using a FE analysis in COMSOL Multiphysics, and are compared with those obtained by using the MT's estimate. At the mesoscale, the average stress components inside a spheroidal inclusion containing distribution of spheroidal voids are compared with those calculated using the multiscale approach, i.e. MT's estimate for the equivalent elastic properties of the porous material combined with the Eshelby's solution for the spheroidal inclusion.

The plan of the paper is the following. Section 2 introduces the microscale analysis proposed by Tandon and Weng in [12] and based on the MT's estimate. In Section 3, Eshelby's fundamental solution is combined with the MT's estimate, to provide a stress analysis of the cluster of degenerated graphite.

Section 4 is devoted to the numerical validation. Some concluding remarks and possible extensions of the hierarchical approach are presented in Section 5.

## 2. Degenerated graphite modelling at the microscale

Consider a composite material in which spheroidal inclusions with an aspect ratio $t$ (the ratio of length to semi-diameter) are uniformly dispersed at random in a three-dimensional isotropic infinite matrix. Due to the random orientations of the inclusions, the composite as a whole is macroscopically isotropic.

By means of Eshelby's equivalent principle and considering the variation of the average stress in the matrix, Tandon and Weng have determined the effective bulk and shear moduli of the equivalent material, cf. Eqns. (22) and (23) in [12]. By using these Equations, the effective bulk and shear moduli can be calculated in terms of the volume fraction of the inclusions, $\lambda$, on their aspect ratio, $t$, and on the elasticity coefficient of the matrix and of the inclusions. Unfortunately, the effective moduli take very long expressions, which have been here omitted for the sake of brevity. In the case of cracks, i.e. for voids with aspect ratio $t$ going to infinity, the effective Young's modulus, $\bar{E}$, and Poisson's ratio, $\bar{\nu}$, take the following simple forms:

$$\bar{E} = \frac{15\,E\,(1-\lambda)}{15+4\lambda(5+\nu-4\nu^2)}, \tag{1}$$

$$\bar{\nu} = \frac{15\nu+\lambda(5-3\nu-8\nu^2)}{15+4\lambda(5+\nu-4\nu^2)}, \tag{2}$$

where $E$ and $\nu$ are the Young's modulus and Poisson's ratio of the matrix, respectively, and $\lambda$ is the volume fraction of voids.

The simplest estimate for the effective elastic behavior of a porous material with porosity λ is given by the classical rule of mixtures:

$$E_{mix} = E\,(1-\lambda), \tag{3}$$

$$\nu_{mix} = \nu\,(1-\lambda). \tag{4}$$

In Section 4, the predictions of the effective composite behavior given by Eqns. (3)-(4) and by the implementation of Eqns. (22) and (23) in [12] on the commercial software Matlab (2019a) are compared with the results of a FE analysis.

## 3. Cluster modelling at the mesoscale

The second step of the multiscale approach considers a cluster of graphite precipitates as a spheroidal inclusion made of a material with elastic properties given Eqns. (22) and (23) in [12]. The inclusion is perfectly bonded to an elastic infinitely extended three-dimensional matrix under a given remote uniform load $\sigma_0$. The goal of the modeling is to calculate the stress components inside the inclusion.

Eshelby proved elegantly that the stress and strain fields inside an ellipsoidal inhomogeneity are uniform, with magnitudes only dependent on the elasticity constants of the inclusion and matrix materials, on the aspect ratio of the ellipsoid, and on the applied remote load [13-15]. In particular, the stress inside the spheroidal inclusion is expressed as

$$\sigma = \sigma_0 - C_0[S-I](S+[C_1-C_0]^{-1}C_0)^{-1}{C_0}^{-1}\sigma_0, \tag{5}$$

where $C_0$ is the elasticity tensor of the material of the matrix, $S$ is the Eshelby's tensor, $I$ is the fourth-order identity tensor, and $C_1$ is the elasticity tensor of the material of the inclusion. The components of the Eshelby's tensor $S$ are given in Appendix 1 of [12]. In the present multiscale model, the elasticity tensor $C_1$ is isotropic, with the elastic moduli of the equivalent porous material analyzed in Section 2.

## 4. Numerical validation of the model

To verify the accuracy of the model, we have tested it against numerical simulations at three different levels: at the microscale, at the mesoscale and at the multiscale.

### *4.1. Validation at the microscale*

In order to verify the accuracy of the analytical model, a three-dimensional FE analysis has been carried out using a commercially available software (COMSOL Multiphysics).

The elastic constants of the matrix are E=206 GPa and ν=0.3. Two types of voids distributions have been examined: an ordered distribution and a disordered distribution. The ordered distribution is characterized by randomly oriented voids placed at the centers of a uniform grid with cube elementary cells of 1x1x1 mm. The union of 6x6x6 elementary cells gives the cube of Figure 1. The voids, in the disordered distribution, have centers placed randomly inside the volume without overlapping as reported in Figure 2. In both types of voids distributions, the internal voids are spheroids with semi-axis ratio ranging between 0.1 and 0.8.

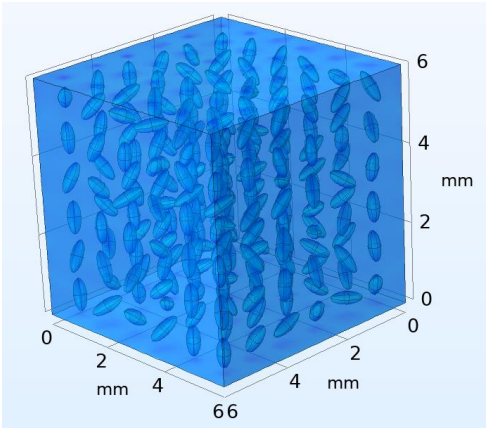


**Figure 1.** Ordered distribution of randomly oriented voids in a cube of 6x6x6 mm

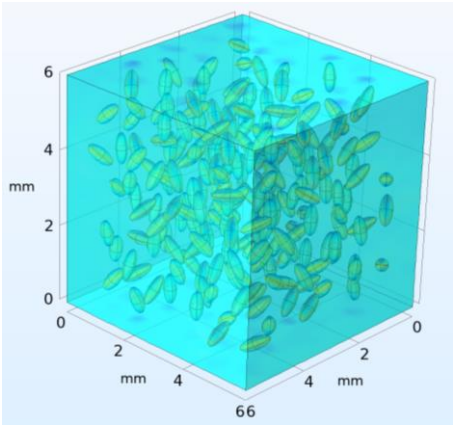


**Figure 2.** Disordered distribution of randomly 216 oriented voids in a cube of 6x6x6 mm

In order to numerically evaluate the effective Young's modulus, $\bar{E}$, and the effective Poisson's ratio, $\bar{\nu}$, a uniform tensile stress $\sigma_n$ was applied along the $z$ direction at $z = L$, whereas the displacement boundary conditions are reported schematically in Figure 3. The average displacements in the z direction $\Delta u_z$ at the surface $z = L$, the average displacements $\Delta u_x$ in the $x$ direction at the free surface $x = L$, and the $\Delta u_y$ in the $y$ direction at the free surface $y = L$ have been calculated. In this way, the Young's modulus will be $\bar{E} = \sigma_n/(\Delta u_z/L)$, and Poisson's ratio results $\bar{\nu}_x = -(\Delta u_x/L)/(\Delta u_z/L)$, and $\bar{\nu}_y = -(\Delta u_y/L)/(\Delta u_z/L)$.

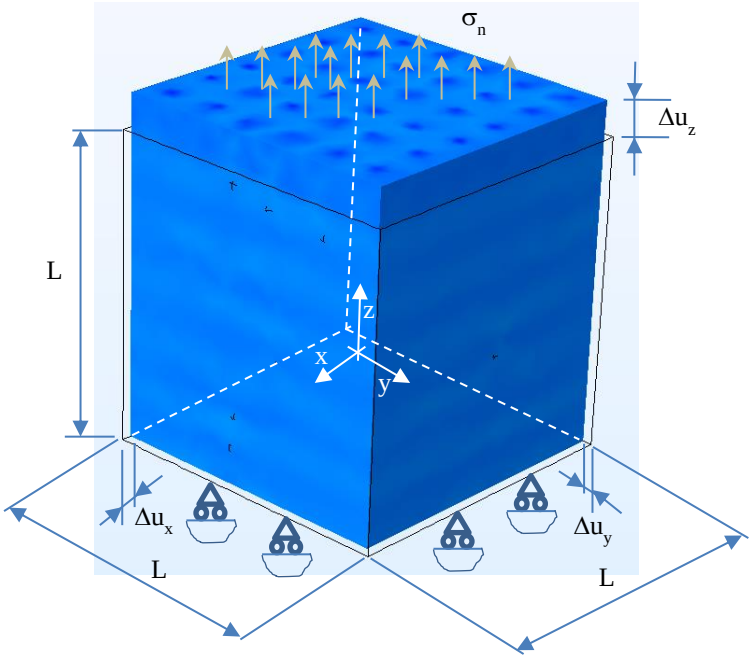


**Figure 3.** Ordered distribution of randomly oriented voids in a cube of LxLxL mm (L=6 mm).

The effective elastic moduli calculated with the FE analysis have been compared with the prediction provided by Eqns. (3), (4) and by Eqns. (22) and (23) in [12]. For ordered distributions of voids, Figures 4 and 5 show the effect of porosity density and voids aspect ratio on the effective normalized Young's modulus, $\bar{E}/E$, and on the effective normalized Poisson's ratio, $\bar{\nu}_x/\nu$, respectively. The symbols, labeled "FE", correspond to the data obtained by the FE analysis; the dashed curves, labeled "TW", are the estimates provided by Tandon and Weng in [12]. In the two figures, the predictions given by the rule of mixture through Eqns. (3) and (4) are also shown (continuous black marked curves). The comparison between the effective elastic moduli computed with the FE simulations (symbols) and with the TW estimates (dashed curves) for disordered void distributions is shown in Figures 6 and 7.

For ordered distributions, the data indicate a very good agreement between the two estimates (FE and TW), with a maximum error of 0.3% for the effective normalized Young modulus, and a maximum error of 8.0% for the effective normalized Poisson's coefficient. The maximum error are reached for a porosity value of 25%, which is higher than typical values of graphite volume fraction in gray cast iron (about 10-15%). For disordered distributions, the Young modulus computed numerically and via the TW estimate are still in very good agreement, with a maximum error of 2% at porosity values of 25%. For the Poisson's coefficient, the agreement is less pronounced, with a maximum error of 24%.

Finally, Figures 4 and 6 indicate that the rule of mixture cannot be considered an acceptable estimate for the effective normalized Young's modulus, providing always an overestimate, with a maximum error of 19% for ordered distributions of voids and of 28% for disordered distributions. For the effective normalized Poisson's ratio, Figures 5 and 7 show that the rule of mixtures always provides an underestimate, with a maximum error of 11% for ordered distributions of voids and of 4% for disordered distributions. These data indicate that the rule of mixture can be considered to provide an acceptable estimate for the Poisson's ratio but not for the Young's modulus.

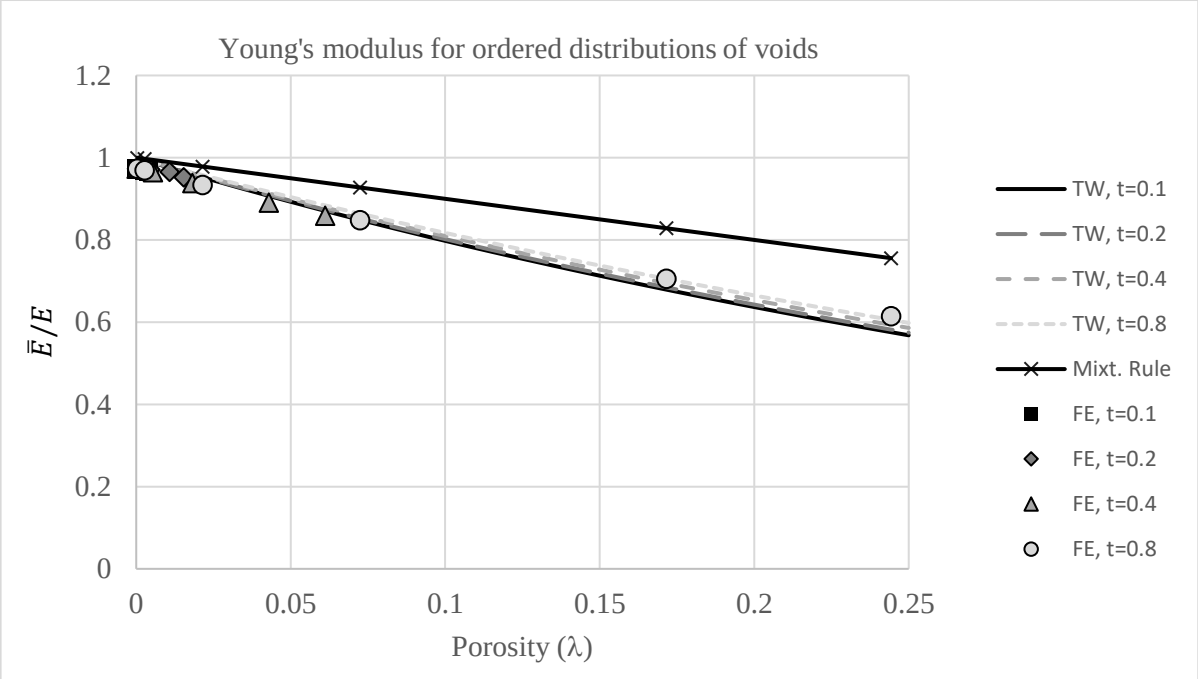


**Figure 4.** Non-dimensional effective Young's modulus versus porosity for ordered distributions of voids. Different void aspect ratios $t$ are considered. Symbols correspond to FE data, dashed curves to the estimate of Tandon and Weng, continuous black marked curve to the rule of mixture.

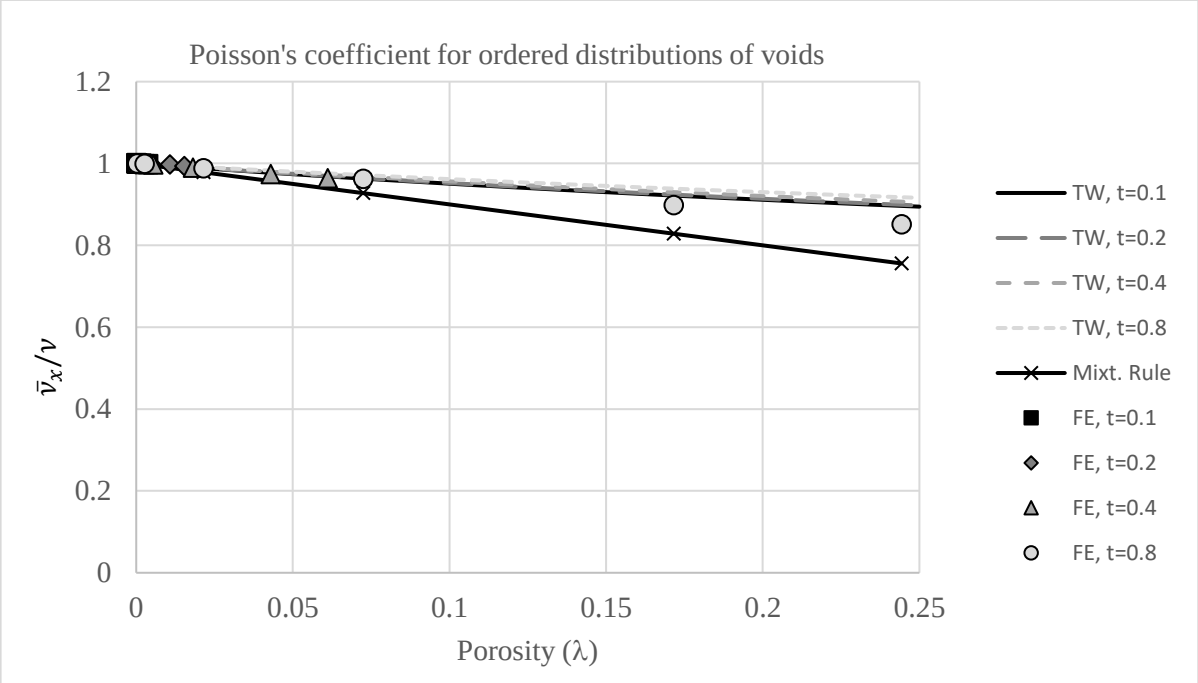


**Figure 5.** Non-dimensional effective Poisson coefficient versus porosity for ordered distributions of voids. Different void aspect ratios $t$ are considered. Symbols correspond to FE data, dashed curves to the estimate of Tandon and Weng, continuous black marked curve to the rule of mixture.

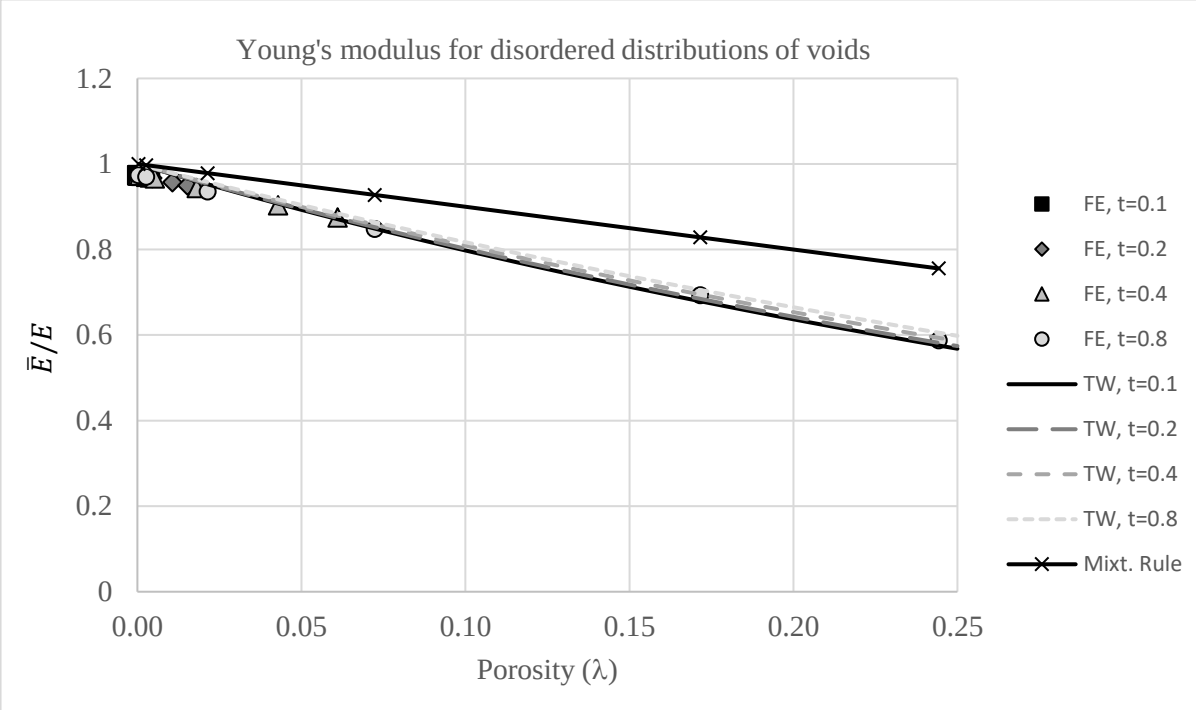


**Figure 6.** Non-dimensional effective Young's modulus versus porosity for disordered distributions of voids. Different void aspect ratios *t* are considered. Symbols correspond to FE data, dashed curves to the estimate of Tandon and Weng, continuous black marked curve to the rule of mixture.

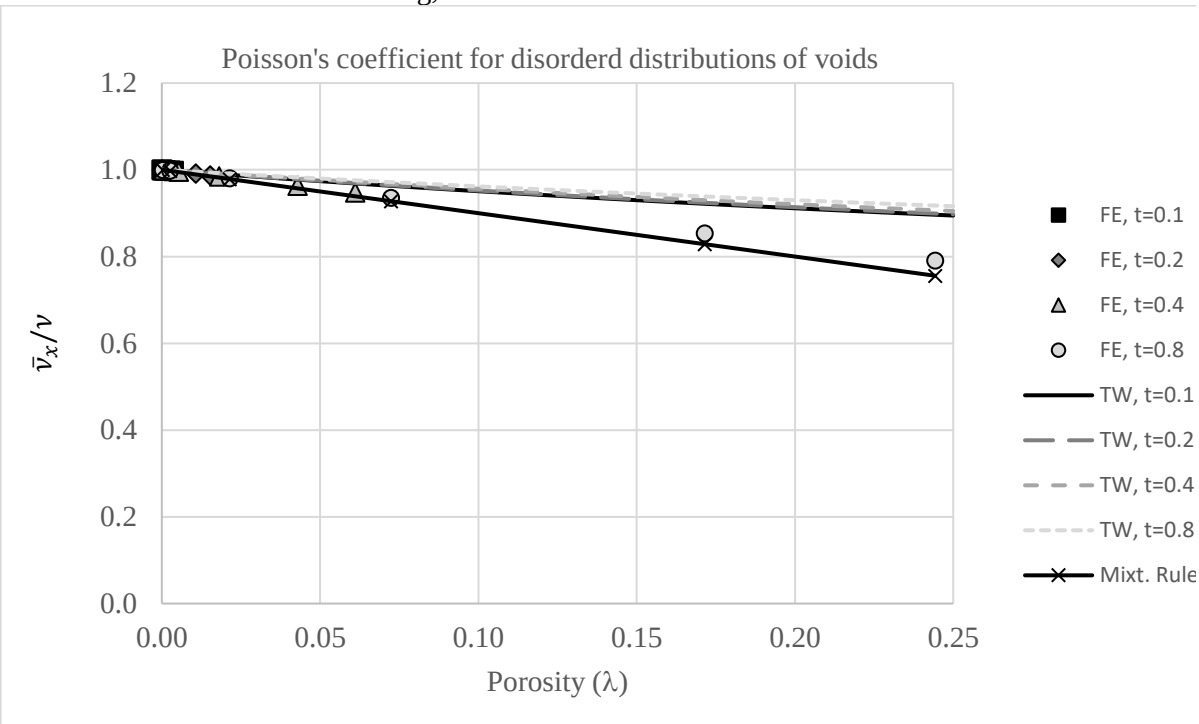


**Figure 7.** Non-dimensional effective Poisson coefficient versus porosity for disordered distributions of voids. Different void aspect ratios *t* are considered. Symbols correspond to FE data, dashed curves to the estimate of Tandon and Weng, continuous black marked curve to the rule of mixture.

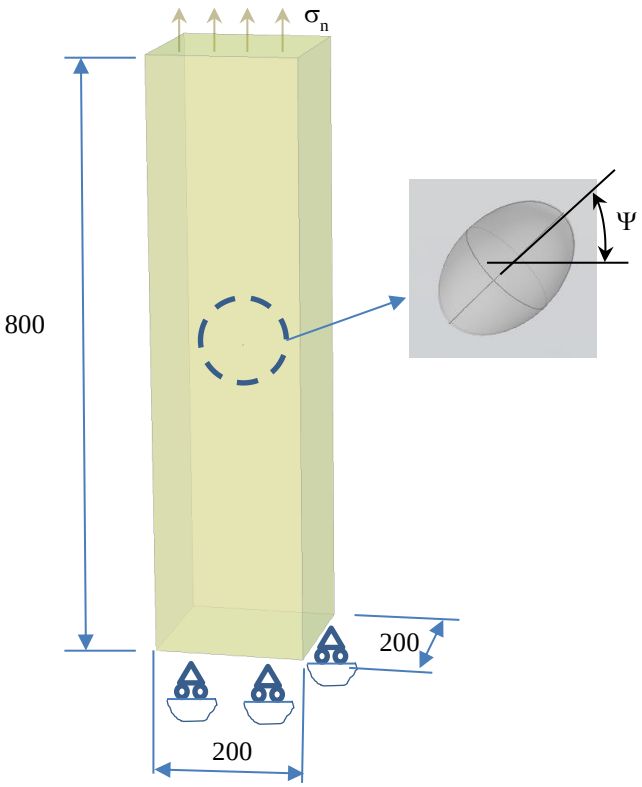


**Figure 8.** Validation at the mesoscale: the ellipsoid inclusion is made of a homogenous isotropic elastic materials with semi axis equal to 1 mm and 1.5 mm.

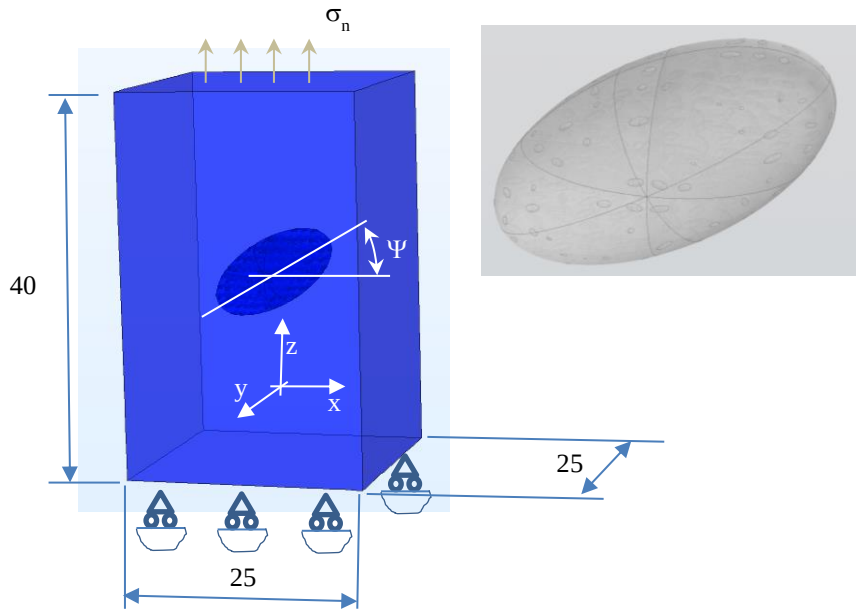


**Figure 9.** Validation at the multiscale: ordered distribution of randomly oriented voids in an ellipsoid of revolution with semi axis equal to 3.5 mm and 7 mm. The internal voids are ellipsoids of revolution with semi axis equal to 0.16 mm and 0.4 mm.

### *4.2. Validation at the mesoscale*

At the mesoscale, we validate the FE analysis against the Eshelby's solution. In both approaches, the inclusion is made of a homogenous isotropic elastic materials, with elastic constants $E_1 = 10$ GPa, $\nu_1 = 0.4$. The elastic constants of the matrix are $E = 206$ GPa, $\nu = 0.3$. An uniaxial traction along the vertical axis has been assigned, and three different orientations $\psi$ of the inclusion with respect to the loading axes, 0°, 30° and 45°, have been assumed, cf. Figure 8. In all cases, the aspect ratio of the cluster has been kept fixed and equal to 1.5. The results, shown in Table 1, indicate an almost perfect agreement between the (constant) stress components calculated analytically by using Eqn. (5) and via FE analysis.

### *4.3 Validation at the multiscale*

To validate the multiscale model, we have considered a porous spheroidal cluster under uniaxial tensile loading, as shown in Figure 9. The cluster, with aspect ratio equal to 2.0, has been taken with two different orientations respect the $(x, y)$ plane, $\psi = 0°, 30°$. Inside the cluster, the ordered porous distributions of voids is characterized by small spheroids with semi axis equal to 0.16 mm and 0.4 mm, respectively. The elastic constants of the matrix are as before, $E = 206$ GPa, $\nu = 0.3$. A FE model was used to analyze the average stress inside the cluster. Figure 8 shows the boundary conditions used in the numerical analysis. Table 2 shows the average values of the stress components inside the cluster calculated with the FE simulation, and the constant stress components obtained by injecting Eqns. (22) and (23) in [12] specialized for voids into Eqn. (5). The data listed in Table 2 indicate an overall good agreement between the two sets of stress components. Because the validation of the FE analysis with the Eshelby's solution provides an almost perfect agreement between stress components inside the cluster starting from the same isotropic material, the lower precision of the multi-scale model in capturing the average stress components in porous inclusions is most probably due to the errors of the Tandon and Weng's approach in estimating the effective elastic moduli of the porous material.

**Table 1.** Validation at the mesoscale: comparison between the two sets of constant stress components calculated and via a FE analysis (label "FE"), and using Eqn. (5) (label "Eshelby"). For the values of the elastic constants of the homogeneous inclusion and of the matrix see text. The angle $\psi$ indicates the orientation of the inclusion, cf. Fig. 8.

| Model | $\psi$ | $\sigma_x$ | $\sigma_y$ | $\sigma_z$ | $\sigma_{xy}$ | $\sigma_{xz}$ |
|---|---|---|---|---|---|---|
| **FE** | 0° | 0.030 | 0.030 | 0.010 | 0.000 | 0.000 |
| **Eshelby** | | 0.030 | 0.030 | 0.010 | 0.000 | 0.000 |
| **FE** | 45° | 0.043 | 0.042 | 0.123 | 0.000 | 0.000 |
| **Eshelby** | | 0.043 | 0.042 | 0.123 | 0.000 | 0.000 |
| **FE** | 90° | 0.058 | 0.053 | 0.145 | 0.000 | 0.000 |
| **Eshelby** | | 0.058 | 0.053 | 0.145 | 0.000 | 0.000 |

**Table 2.** Full validation of the multiscale model: comparison between the two sets of constant stress components calculated via a FE analysis (label "FE"), and using Eqn. (5) coupled with Eqns. (22) and (23) in [12] specialized for voids (label "MM"). For information on the microstructure parameters see text. The angle $\psi$ indicates the orientation of the inclusion, cf. Fig. 9.

| Model | $\psi$ | $\sigma_x$ | $\sigma_y$ | $\sigma_z$ | $\sigma_{xy}$ | $\sigma_{xz}$ |
|---|---|---|---|---|---|---|
| **FE** | 0° | 0.000 | –0.002 | 0.969 | 0.000 | 0.000 |
| **MM** | | –0.003 | –0.003 | 0.947 | 0.000 | 0.000 |
| **FE** | 30° | –0.002 | –0.002 | 0.966 | 0.000 | –0.003 |
| **MM** | | –0.003 | –0.002 | 0.953 | 0.000 | –0.004 |

## 5. Conclusions

In this paper, we have proposed a three-dimensional multi-scale model for the stress analysis inside a cluster of degenerated graphite in grey cast iron. The graphite precipitates are viewed as voids embedded in a three-dimensional infinite elastic matrix. A cluster of graphite precipitates is viewed as a spheroidal inclusion, whose elastic properties are calculated by using the Tandon and Weng's estimate for porous materials. In the proposed multi-scale approach, the (average) stress components inside the cluster are found to depend on the following microstructure parameters:

- graphite density, here modeled as a porosity density;
- graphite aspect ratio, i.e. the void aspect ratio;
- the orientation of the cluster;
- the aspect ratio of the cluster.

To validate the multi-scale model, we have performed a numerical validation at the microscale, i.e. at the scale of the graphite precipitates, and at the mesoscale, i.e. at the scale of the graphite clusters. The validation at the microscale shows a good agreement between the equivalent elastic properties of the porous material calculated via the FE simulations and the effective elastic constants calculated using the approach by Tandon and Weng.

The validation at the mesoscale shows an almost perfect agreement between the stress components inside a homogeneous inclusion calculated via a FE simulation and using Eshelby's. The validation obtained coupling the microscale with the mesoscale shows a good agreement between the stress components inside a porous cluster calculated via FE analysis and using the multi-scale model. The lower precision with respect to the validation of FE data against the Eshelby's solution is probably due to the propagation of errors arising from the estimate of the Tandon and Weng's approach at the microscale.

Future developments of the present model may address the prediction of damage internal to the cluster on the basis of the estimated stress components. Other issues to be explored could be the bonding and the damage of the graphite particles at the interface with the matrix, cf. [17-20].

## References

[1] Hütter G, Zybell L and Kuna M 2015 *Eng. Fract. Mech.* **144** 118
[2] Rausch T, Beiss P, Broeckmann C, Lindlohr S and Weber R 2010 *Procedia Eng.* **2** 1283
[3] Costa N, Machado N and Silva F 2010 *Int. J. Fatigue* **32** 988
[4] Lacaze J, Asenjo I, Mendéz S, Sertucha J, Larranaga P and Suárez R 2012 *Int. J. Metalcasting/Winter* 35.
[5] Kaczorowski J, Jozwiak K and Innocenti M 2013 *J. Fail. Anal. Prev.* **13** 445
[6] Boccaccini A R 1997 *Z. Metallkd* **88** 23
[7] Gaudig W, Mellert R, Weber U and Schmauder S 2003 *Comput. Mater. Sci.* **28** 654
[8] Sjögren T and Svensson I L 2004 *Int. J. Cast Met. Res.* **17** 271
[9] Svensson I L and Sjögren T 2009 *Int. J. Metalcast.* **3** 67
[10] Cova M, Livieri P, Rizzoni R and Tovo R 2017 *Procedia Struct. Integrity* **7** 446
[11] Rizzoni R, Livieri P, Tovo R and Cova M 2020 *Theor. Appl. Fract. Mech.* https://doi.org/10.1016/j.tafmec.2020.102731 in press
[12] Tandon G P and Weng G J 1986 *Compos. Sci. Tech.* **27** 111
[13] Eshelby J D 1957 *P. Roy. Soc. A-Math. Phy*. **241** 376
[14] Eshelby J D 1959 *P. Roy. Soc. A-Math. Phy*. **252** 561
[15] Eshelby J D 1961 *Progress in Solid Mechanics*, eds. N Sneddon and R Hill (Amsterdam: North-Holland) vol. 2 89–140. Amsterdam: North-Holland
[16] Ju J W and Sun L Z 1999 *Trans. ASME* **66** 570.
[17] Lebon F, Dumont S, Rizzoni R, López-Realpozo J C, Guinovart-Díaz R, Rodríguez-Ramos R, Bravo-Castillero J and Sabina F J 2016 *Compos. Part B-Eng*. **90** 58
[18] Bonetti E, Bonfanti G, Lebon F and Rizzoni R 2017 *Meccanica* **52** 1911
[19] Guinovart-Sanjuán D, Rizzoni R, Rodríguez-Ramos R, Guinovart-Díaz R, Bravo-Castillero J,

Alfonso-Rodríguez R, Lebon F, Dumont S, Sevostianov I and Sabina F J 2017 *Compos. Struct.* **176** 539
[20] Livieri P and Tovo R 2017 *Int. J. Fatigue* **101** 363